Unraveling the impact of temperature on the reaction kinetics of the electro-oxidation of methanol on Pt(1 0 0)

Enrique A. Paredes-Salazar [a,b], Alfredo Calderón-Cárdenas [c], Enrique Herrero [b,*], Hamilton Varela [a,*]

[a] São Carlos Institute of Chemistry, University of São Paulo, P. O. Box 780, CEP 13560-970 São Carlos, SP, Brazil
[b] Instituto de Electroquímica, Universidad de Alicante, Apdo. 99, E-03080 Alicante, Spain
[c] GIFBA, Universidad de Nariño, 520002 San Juan de Pasto, Nariño, Colombia

ABSTRACT

Methanol is one of the key molecules in the challenge towards a sustainable future, particularly as a renewable hydrogen carrier fuel and as a low-carbon and net carbon-neutral liquid chemical. For most applications, it is imperative to understand the impact of temperature on the methanol electro-oxidation reaction (MEOR). In this study, the influence of the temperature on the kinetics of the MEOR and the parallel reaction pathways is assessed by investigating responses in both conventional and oscillatory regimes using a single-crystal Pt(1 0 0) electrode. Our findings demonstrate that chronoamperometric measurements under steady-state conditions provide more reliable values for apparent activation energies compared to transient conditions. Furthermore, a temperature-dependent shift in the dominance of specific oxidation pathways is observed, analogous to a kinetic and thermodynamic control mechanism, preventing the complete poisoning of the electrode surface. Specifically, oxidation pathways leading to the formation of reaction byproducts predominate at lower temperatures, while the oxidation pathway via CO_{ad} becomes dominant at temperatures exceeding 30 °C. Moreover, our research shows that, at shorter times, temperature changes minimally affect the mean potential required to sustain the applied current during the oscillations in a galvanostatic experiment, which is closely linked with the voltaic efficiency. However, over longer periods, when mass transport phenomena become significant and mixed-mode oscillations occur, elevated temperatures increase the mean potential, resulting in reduced voltaic efficiency. Therefore, to facilitate the complete conversion of methanol to CO_2 without increasing the mean potential for current maintenance, it is essential not only to increase the temperature but also to improve the mass transport conditions to mitigate the mixed-mode oscillations, despite their lower minima reached during oscillation. This idea challenges the conventional assumption that a lower minimum potential implies a lower mean potential during oscillations. This advancement propels our understanding to a more sophisticated level, providing valuable insights to guide the materials design to increase the conversion efficiency and optimize the operating temperature of devices crucial to energy conversion.

1. Introduction

The transition from our current energy sector towards a sustainable and environmentally friendly scenario, characterized by reduced reliance on fossil fuels and substantial reductions in air pollution emissions, needs the transformation of abundant atmospheric molecules such as H_2O, N_2, and CO_2 into usable fuels or fuel precursors like H_2, NH_3, and $C_xH_yO_z$ (hydrocarbons) [1]. Among these potential products, methanol stands out as a key player, particularly when obtained from sustainable

biomass or captured CO_2 [2] and H_2 supplied from renewable electricity, commonly referred to as bio-methanol and e-methanol, respectively [3]. A common usage is in the so-called direct methanol fuel cells (DMFCs) [4–9], through which electrical energy can be generated with remarkable theoretical efficiency [7,10], establishing a sustainable energy cycle. Furthermore, the methanol electro-oxidation reaction (MEOR) offers an intriguing alternative to the oxygen evolution reaction (OER) in the anodic compartment of electrochemical reforming devices for green hydrogen production via electrolysis [11,12]. This substitution

results in a lower thermodynamic potential for hydrogen production, aligning with the aspirations of a green economy. However, the feasibility of these approaches depends on several factors, including the resolution of specific electrochemical issues, such as the development of efficient and selective catalysts at each stage. These catalysts must exhibit the capability to convert reactants into desired products with high efficiency at low overpotentials [1].

Platinum-based materials are widely employed as electrocatalysts for the MEOR due to their exceptional properties to increase the known sluggish kinetics of the oxidation of small organic molecules [13]. However, at low potentials, the electrode surface becomes predominantly poisoned by the adsorbed carbon monoxide (CO_{ad}) intermediate, effectively hindering the reaction progress [14–16]. Furthermore, the formation of reaction byproducts that exchange fewer electrons per oxidized methanol molecule than the complete oxidation to CO_2, specifically formaldehyde, methyl formate, and formic acid, results in reduced conversion efficiency [4,7,8,15,17,18]. Therefore, it is imperative to gain a comprehensive understanding of how the reaction occurs and how it is influenced by various reaction conditions. Such knowledge is essential to identify the specific features of the electrocatalyst that can boost reaction kinetics and increase its selectivity. The final goal is to favor the production of CO_2 while preventing electrode surface poisoning, a critical aspect in the development of catalytic materials.

Deciphering molecular reactions implies understanding the intricate interplay between the electrode surface and reaction intermediates and how this interplay governs the reaction rates and catalytic activity. This requires bridging the microscopic description of each elementary reaction with the laboratory-scale kinetic descriptors, *i.e.*, the electrochemical response recorded during the reaction [19]. Electrochemical responses observed under both stationary and transient conditions are instrumental in studying systems like the MEOR and electrochemical systems in general. They offer complementary insights into the phenomena occurring at the electrode interface [20]. Moreover, under various experimental conditions, encompassing potential control and current control settings, the electrochemical response can manifest spontaneous oscillatory behavior [21,22]. These oscillations have demonstrated greater sensitivity to environmental variables compared to the response observed through conventional regimes [23,24], rendering them a reliable tool for assessing interfacial phenomena and the impact of experimental conditions on them [25,26]. Importantly, the oscillatory behavior arises naturally in complex systems [21,22], including the MEOR on Pt electrodes, and does not require periodic perturbations to induce it. For instance, in a galvanostatic experiment, where a constant applied current is maintained, the measured potential oscillates due to the inherent interaction of at least two processes, one autocatalytic and one autoinhibition process [21,22]. This interaction results in periodic changes in the electrode surface coverage by blocking species. Specifically, while greater coverages result in a higher potential necessary to maintain the applied current, this potential diminishes when surface sites are liberated [25].

Additionally, the use of monocrystalline electrodes provides an advantageous and precise means of correlating the electrochemical response with the electrode surface [27,28]. Their controlled atomic arrangement on the surface results in a uniform distribution of active sites which facilitates a precise correlation between electrocatalytic properties and surface structure [27,28]. Among the low-index single-crystal platinum electrodes, the Pt(1 0 0) plane stands out for its remarkable activity at higher potentials [29,30], a critical region where the MEOR extends beyond electrode poisoning. Furthermore, on this surface, oscillations during the MEOR span a broader potential range, enabling the comprehensive study of various processes occurring throughout the reaction [23]. In this regard, the electrochemical response recorded under oscillatory regimes during the MEOR on a Pt (1 0 0) electrode serves as a powerful and sensitive tool for gaining valuable insights into the reaction mechanism and how it responds to different conditions.

This information is particularly relevant in the context of fuel cells and electro-reforming devices utilizing methanol, where temperature is a critical parameter that significantly affects the reaction kinetics. Consequently, any changes in the reaction mechanism, *i.e.*, on the main reaction pathways, must be taken into account when designing materials for future applications and optimizing the operating parameters of DMFCs [6]. Numerous studies have focused on determining the apparent activation energy as a key kinetic parameter to identify rate-limiting steps over a specific temperature range. However, the value of this kinetic parameter can vary substantially depending on both the applied potential and the experimental setup [10]. Consequently, establishing an accurate correlation between the measured activation energy value and the reaction step governing the reaction kinetics has proven challenging [10]. In this study, we contribute to the elucidation of how temperature impacts the main reaction pathways using the electrochemical response under conventional and oscillatory conditions on a Pt(1 0 0) electrode, with a particular emphasis on the latter. This underscores the potential applicability of oscillatory behavior for assessing electrocatalytic reactions and providing crucial insights for catalyst development and optimization.

2. Experimental section

2.1. Electrochemical measurements

All electrochemical measurements were conducted using a conventional three-electrode cell in a non-isothermal configuration. A large Pt wire served as the counter electrode, while a reversible hydrogen electrode (RHE) was used as the reference electrode. The RHE was prepared in the same supporting electrolyte, and to which all potentials are referred. The Pt(1 0 0) working electrode was prepared from a single-crystal platinum bead with a diameter of *ca.* 2.5 mm. The preparation procedure followed the methods described in reference [31]. Prior to each measurement, the electrode was cleaned using the flame annealing technique and then cooled in an atmosphere containing a mixture of H_2/ Ar. To prevent contamination during the transfer of the electrode to the controlled atmosphere of the cell, the surface was protected with a droplet of ultrapure water in equilibrium with the cooling atmosphere [31]. The working electrode was immersed in the cell in the hanging meniscus configuration maintaining a controlled potential of 0.10 V.

The electrochemical cell was immersed in a water bath, whose temperature was controlled using a Haake FK thermostat. The temperature in the water bath was varied at 5 °C intervals from 10 to 35 °C. In this configuration, temperature variations only affect the electrolyte solution containing the working and counter electrodes, while the reference electrode, which is kept external to the cell and connected through a Luggin capillary, is maintained at room temperature. 0.5 mol L^{-1} $HClO_4$ and 0.5 mol L^{-1} $HClO_4$ + 0.5 mol L^{-1} methanol aqueous solutions were prepared using perchloric acid (70 %, Merck suprapure), methanol (Merck suprapure), and ultrapure water (Milli-Q, 18.2 MΩ cm). Before each experiment, the solution was purged with argon (99.998 %) to remove any dissolved oxygen and then, the gas was placed as surface gas flow throughout the experiment. The gas flow rate was adjusted to the minimum level that would prevent the contribution of the oxygen reduction reaction (ORR) in order to control the mass transfer phenomena and ensure the reproducibility of the experiments, as stated in a previous work [23].

The electrochemical experiments were performed using an Autolab potentiostat/galvanostat PGSTAT 128 N. For all experiments, the cleanliness of the system and the quality of the electrode surface were checked by the characteristic voltammetric profile of the Pt(1 0 0) electrodes in the absence of methanol (Inset in Fig. 1(a)). Cyclic voltammetry (CV) measurements were performed from 0.05 V to 0.80 V at a scan rate of 0.05 V s^{-1} in the supporting electrolyte and from 0.05 V to 0.85 V at 0.01 V s^{-1} in the solution containing methanol. Chronoamperometric experiments were carried out by initially setting the
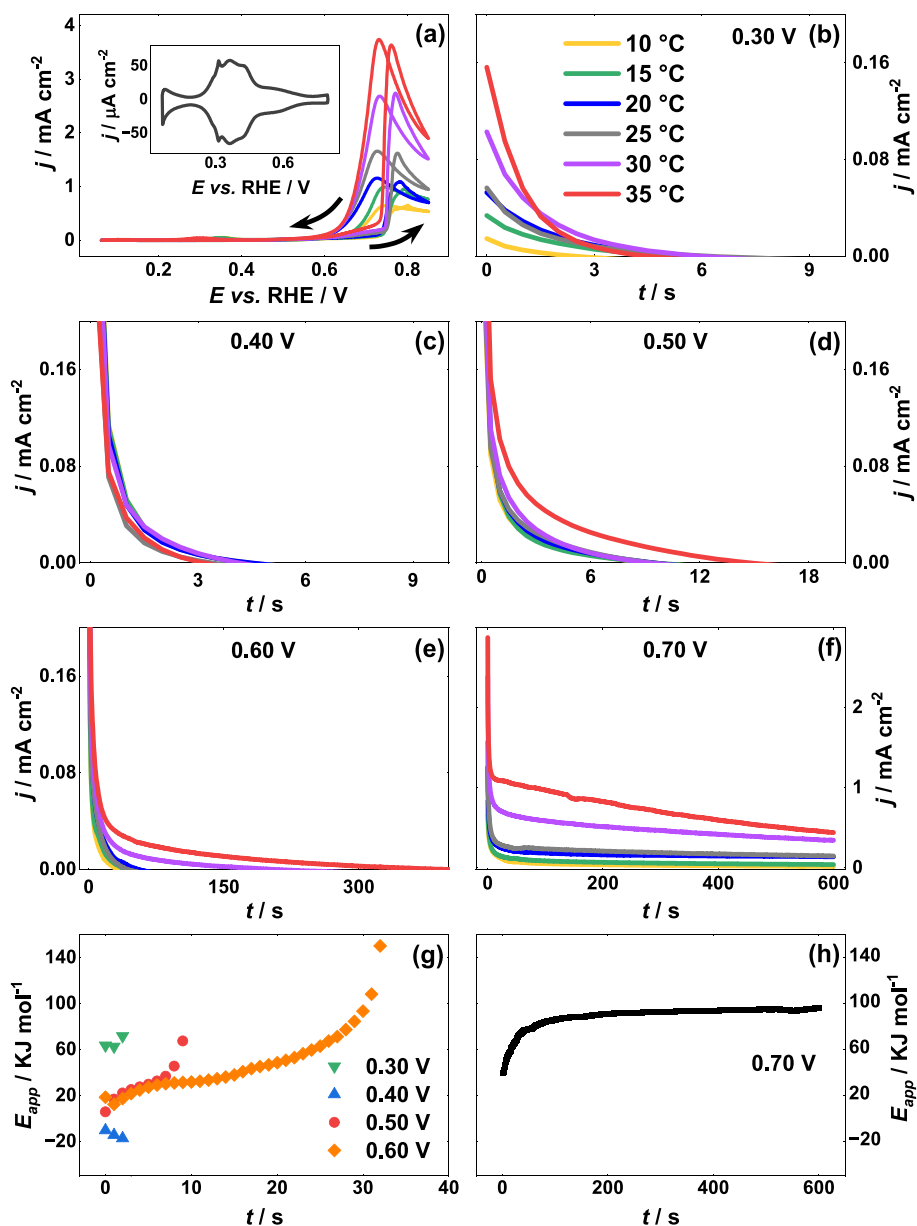
Fig. 1. (a) First cycle in the voltammetric profiles of Pt(1 0 0) in 0.5 mol L^{-1} HClO$_4$ + 0.5 mol L^{-1} CH$_3$OH at different temperatures, scan rate: 10 mV s^{-1}. Inset figure corresponds to the voltammetric profile of the Pt(1 0 0) electrode in the absence of CH$_3$OH, scan rate: 50 mV s^{-1}; (b – f) chronoamperometric curves from 0.30 to 0.70 V on Pt(1 0 0) in 0.5 mol L^{-1} HClO$_4$ + 0.5 mol L^{-1} CH$_3$OH at different temperatures (prior to the 600 s potential step, the electrode was first held at 0.80 V for 2 s, followed by a potential step of 0.10 V for 1 s); (g) time-evolution of the apparent activation energy after applying potential steps of 0.30–0.60 V, and (h) time-evolution of the apparent activation energy after applying potential step of 0.70 V.

electrode potential at 0.80 V for 2 s, followed by a potential step to 0.10 V for 1 s. From this point, the potential was shifted to the desired potential value and maintained for 600 s. The galvanodynamic experiments were performed at a scan rate of 2.0 μA s^{-1} cm^{-2}, starting from an initial current density value of 9.5 × 10^{-5} A cm^{-2} until a value at which the measured electrode potential rose above 1.0 V. Galvanostatic experiments involved applying a potential value of 0.80 V for 2 s, followed by a potential step to 0.10 V for 1 s. Subsequently, the desired current value was applied in each experiment. The pre-treatments of the electrode were devised to ensure that its surface begins the experiments in a state relatively devoid of adsorbed species. Specifically, an initial potential of 0.80 V is selected to facilitate the oxidation of CO$_{ad}$ species, striking a delicate balance between efficient removal and avoiding surface oxidation to maintain the integrity of the single crystal electrode. Subsequently, the potential is adjusted to 0.10 V for 1 s to reduce the

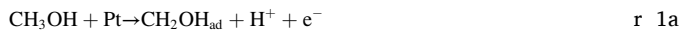adsorbed OH (OH$_{ad}$) species while preventing the oxidative adsorption of methanol.

3. Results and discussion

3.1. Apparent activation energies: conventional regime experiments
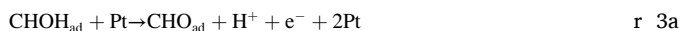
Electrochemical measurements in the non-isothermal configuration may cause the emergence of a thermodiffusion potential due to temperature differences between the working and reference electrodes [32]. In this study, the temperature difference between the reference and working electrodes was limited to a maximum of 15 °C, resulting in thermodiffusion potentials below 6 mV [32]. Given the negligible impact of this small value on the electrochemical response, we considered it acceptable to neglect correction for all measurements. To

facilitate subsequent discussions regarding the temperature's influence on the main reaction pathways of the MEOR, Scheme 1 illustrates the proposed reaction mechanism, previously validated through microkinetic modeling [25]. The reaction steps are enumerated below:
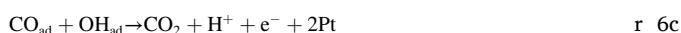
CH$_3$OH oxidative adsorption:

$$CH_3OH + Pt \rightarrow CH_2OH_{ad} + H^+ + e^- \qquad r\ 1a$$

HCO$_{ad}$ formation – Dehydrogenation pathway:

$$CH_2OH_{ad} + Pt \rightarrow CHOH_{ad} + H^+ + e^- \qquad r\ 2a$$

$$CHOH_{ad} + Pt \rightarrow CHO_{ad} + H^+ + e^- + 2Pt \qquad r\ 3a$$

HCO$_{ad}$ formation – Formaldehyde pathway:

$$CH_2OH_{ad} \rightarrow HCHO + H^+ + e^- + Pt \qquad r\ 2b$$

$$HCHO + Pt \rightarrow CHO_{ad} + H^+ + e^- \qquad r\ 3b$$

CO$_2$ formation - Carbon monoxide pathway:

$$CHO_{ad} + Pt \rightarrow CO_{ad} + H^+ + e^- + Pt \qquad r\ 4c$$

$$H_2O + Pt \rightleftharpoons OH_{ad} + H^+ + e^- \qquad r\ 5c, r\ -5c$$

$$CO_{ad} + OH_{ad} \rightarrow CO_2 + H^+ + e^- + 2Pt \qquad r\ 6c$$

HCOOH formation - Dehydrogenation pathway:

$$CHO_{ad} + H_2O \rightarrow CH(OH)OH_{ad} \qquad r\ 4a$$

$$CH(OH)OH_{ad} \rightarrow HCOOH + H^+ + e^- + Pt \qquad r\ 5a$$
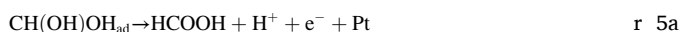
HCOOH formation – Methylformate pathway:

$$CHO_{ad} + CH_3OH \rightarrow CH_3OCHOH_{ad} \qquad r\ 4d$$

$$CH_3OCHOH_{ad} \rightarrow CH_3OCHO + H^+ + e^- + Pt \qquad r\ 5d$$

$$CH_3OCHO + H_2O \rightleftharpoons HCOOH + CH_3OH \qquad r\ 6d, r\ -6d$$
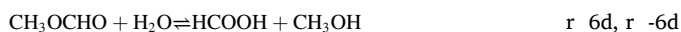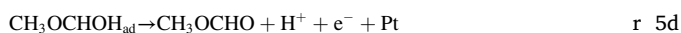
CO$_2$ formation – Formic acid oxidation pathway:

$$HCOOH + 2Pt \rightleftharpoons HCOO_b + H^+ + e^- \qquad r\ 6a, r\ -6a$$

$$HCOO_b + 2Pt \rightarrow HCOO_m + 3Pt \qquad r\ 7a$$

$$HCOO_m + Pt \rightarrow CO_2 + H^+ + e^- + 2Pt \qquad r\ 8a$$

$$HCOO_m + H^+ + e^- + 2Pt \rightarrow CO_{ad} + H_2O + 2Pt \qquad r\ 8e$$
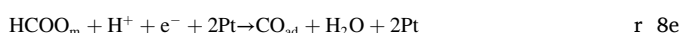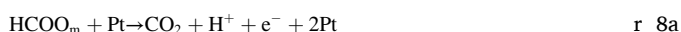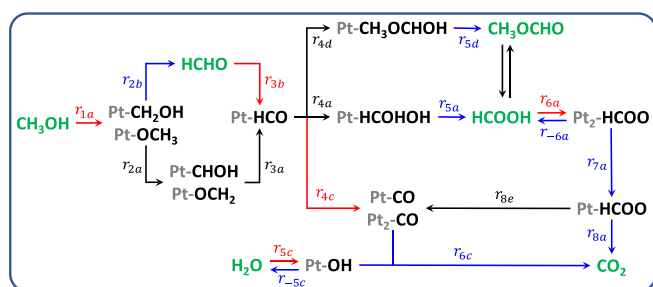
Fig. 1(a) illustrates CV profiles for the MEOR on a Pt(100) electrode at different temperatures. In general, during the positive direction scans, a

Scheme 1. Proposed reaction scheme for the MEOR on Platinum. Species in solution are shown in green, while adsorbed species are shown in black. Red arrows represent steps that consume surface sites, blue arrows represent steps that release surface sites, and black arrows represent steps that neither release nor consume surface sites. Adapted from references [25] and [34].

small peak emerges at *ca.* 0.30 V corresponding to methanol oxidative adsorption [33] (r_{1a}) (Figure S1 in the supplementary information (SI)), a potential value that coincides with the onset of OH species adsorption on Pt(100) electrodes [34–36]. At approximately 0.73 V, the current density shows a sharp increase, reaching its peak between 0.76 and 0.79 V. This characteristic behavior is typical of the MEOR and is primarily associated with the formation of surface poisons, mainly CO$_{ad}$ species, at low potential values. These CO$_{ad}$ species then react with OH$_{ad}$ species (r_{6c}) at high rates at potentials above 0.73 V, leading to an abrupt increase in the current density. In this peak at 0.76 V, CO$_{ad}$ is oxidized, liberating surface sites and allowing direct methanol oxidation to proceed [20,34,37,38]. Above 0.80 V the current decays due to the formation of a compact OH$_{ad}$ layer that prevents the adsorption of methanol. During negative direction scans, broader peaks compared to the positive direction scans are observed within the potential range of 0.73 to 0.75 V. Conversely to positive direction scan, in this case, the electrode surface initially possesses a high fraction of available sites, which gradually becomes poisoned as the potential decreases. This phenomenon results in a slower decrease in current density and the observed broadening of peaks [20,34,37,38]

Above a potential threshold of *ca.* 0.63 V (Fig. 1(a)), it becomes evident that temperature changes have a substantial influence on the current density, with higher temperatures corresponding to increased current density values. Furthermore, an increase in the temperature induces a shift in the peak potential towards lower values. In the case of positive direction scans, this shift is approximately −1.6 mV per degree Celsius, a value consistent with reports for a polycrystalline platinum surface in an acidic medium [10]. The shift of the peak potential towards lower values can be primarily attributed to increased turnover rates of reaction steps involving carbonaceous intermediates, including methanol dehydrogenation and subsequent steps, and to the reduced temperature sensitivity of the OH$_{ad}$ species formation on the Pt(100) surface [39]. Therefore, since the formation rate of OH$_{ad}$ species does not experience a significant rise at higher temperatures, these species are more rapidly consumed during the reaction step involving the oxidation of CO$_{ad}$ species (r_{6c}), which occurs at higher rates as temperature increases. This, in turn, not only leads to an overall increase in the total current with rising temperature but also results in the peak shifting to lower overpotentials.

The activation energy is a fundamental parameter in studying the dependence of the reaction rate on the temperature and comparing the intrinsic activity of different catalysts [40,41]. For multi-step reactions and when it is derived from experimental measurements at different temperatures, it is known as the apparent activation energy (E_{app}). However, it is essential to acknowledge that its experimental determination assumes that variations in temperature induce purely kinetic effects [10,40]. In practice, several factors influence the experimental current density, including the applied potential and processes that may reduce the electrochemically active surface area (*e.g.*, adsorption of reaction intermediates, anions, and oxide formation) [10,40]. Therefore, it is imperative to consider these factors, along with the experimental conditions and methodology, when interpreting E_{app} values and their correlation with surface processes. Some authors have suggested using the negative direction scan, which involves moving from high to low potentials during linear sweep voltammetry, as an approach to mitigate surface poisoning issues and to ensure control over the initial electrode surface conditions, *i.e.*, starting from one free of adsorbed carbonaceous species [10]. However, it is important to note that the scan rate used in potentiodynamic experiments usually influences the oxidation and adsorption processes differently. This can lead to voltammetric profiles and, consequently, E_{app} values that may correspond to a process distinct from that of the MEOR.

To facilitate meaningful comparisons, the uniformity of initial conditions across all voltammetric experiments was ensured by flame annealing the electrode and immersing it in the electrolyte at a

controlled applied potential of 0.10 V before each measurement. This practice guarantees that the results of the positive direction scans are directly comparable. Notably, the CV profiles in Fig. 1(a) show that at potentials below 0.60 V, the differences in current density values during the positive direction scans are negligible. This observation suggests that changes in temperature until 35 °C cannot activate the electron transfer within this specific potential range. Consequently, the calculation of E_{app} at these potentials could introduce substantial errors and may not accurately represent any rate-determining step in the MEOR. In this sense, for comparative purposes, the current density values obtained during the positive and negative direction scans at 0.60 and 0.70 V to determine the E_{app} were selected. During the positive direction scan, the resulting E_{app} values were determined to be 23 ± 2 and 46 ± 3 kJ mol^{-1}, while the current densities of the negative direction scan yield E_{app} values of 37 ± 5 and 58 ± 7 kJ mol^{-1}, respectively. The error for each value was calculated using the standard error of the slope in the Arrhenius plots (Figure S2 in the SI), which were determined through linear regression analysis. The differences in the E_{app} values obtained in the positive and the negative direction scans have been previously demonstrated and are attributed to the accumulation of intermediates that poison the electrode surface [10]. It should be noted that the calculated values of E_{app} do not provide a direct measure of the activation energy for the conversion of methanol to CO_2, but rather reflect the combined influence of several steps occurring simultaneously at these potentials, such as the formation of partial oxidized products and any previous step. These results will be discussed later in context with the E_{app} values determined by chronoamperometry (CA).

In Fig. 1(b-f), chronoamperometric profiles recorded at potentials from 0.30 to 0.70 V at different temperatures are presented. For all applied potentials except 0.70 V, the current density gradually approaches zero as time progresses. To understand this behavior, it is essential to consider the controlled initial conditions of the electrode surface, achieved by applying a potential of 0.80 V, followed by a potential step of 0.10 V before reaching the target potential. Furthermore, the use of $HClO_4$ as a supporting electrolyte allows for neglecting the adsorption of anions. Consequently, the gradual decay in current density towards zero can predominantly be attributed to surface poisoning, particularly by CO_{ad} [20,42]. Within this potential range (0.30 to 0.60 V), the influence of temperature on the magnitude of current density is minimal. Increases in temperature are associated with slight increases in current density, while the primary effect of temperature becomes apparent with increasing the time required for the current density to reach zero. This observation implies that, to some extent, higher temperatures accelerate the rate of certain reactions within the reaction mechanism and delay the total surface poisoning. These processes may include oxidative adsorption and dehydrogenation of methanol (r_{1a}, r_{2a}, r_{3a}, r_{2b}, r_{3b}), resulting in the formation of partially oxidized products, predominantly CO_{ad}. However, higher overpotentials are critical in overcoming the activation energy of the rate-determining step and preventing electrode poisoning. These results are consistent with the observations from the CV profiles previously discussed, where small current densities and minimal temperature-induced variations were observed at potential values lower than 0.60 V, further confirming that temperature has minimal effect on the reaction kinetics associated with surface poisoning species in this potential range.

The calculation of E_{app} values within the potential range of 0.30 and 0.60 V could be attempted using current densities measured at short times during the CAs. During this brief period, the electrode surface has not yet become completely poisoned, resulting in current densities discernible from zero. However, it is important to acknowledge that determining E_{app} in this manner results in values that represent a complex convolution of various transient processes that lead to the formation of surface poisons, primarily CO_{ad} as already mentioned, exhibiting temperature-dependent kinetics and contributing to subtle variations in the current density. Nonetheless, relying on such calculations to derive

representative values for the overall process at these potentials is problematic. Numerical simulations have revealed that, during the transient, the contribution of each reaction step to E_{app} fluctuates dynamically and an increase in the total current density does not necessarily correlate with a decrease in the apparent activation energy [40]. Additionally, E_{app} may evolve over time until the system reach the steady state. This evolution can sometimes results in negative values, potentially introducing large errors in its interpretation [40]. Consequently, relating calculated E_{app} values during the transient to specific steps within the reaction mechanism, especially those exerting a significant influence on the overall reaction rate, becomes a major challenge. Therefore, it is advisable to determinate the E_{app} under steady-state conditions to ensure more reliable results.

To illustrate this point, Fig. 1(g) depicts the temporal evolution of the E_{app} within the potential range of 0.30 to 0.60 V during the time interval when non-zero current densities are recorded. This plot clearly illustrates the sudden variations in the E_{app} values under these conditions, where a steady state has not yet been reached, even taken negative values at 0.40 V, as has been demonstrated in previous numerical experiments [40]. In contrast, the current densities recorded in CAs at 0.70 V eventually stabilize at non-zero steady-state values at extended time intervals (*cf.* Fig. 1(f)). This behavior results in an asymptotic increase in E_{app} values over time until a constant value is ultimately reached. To reconcile the E_{app} values obtained from positive direction scans during CVs at 0.60 V and 0.70 V (23 ± 2 and 46 ± 3 kJ mol^{-1}), E_{app} must be determined at 5 s after the potential step. This determination yields E_{app} values of 27 ± 3 and 47 ± 6 kJ mol^{-1}, respectively. For the negative direction scans, which gave values of 37 ± 5 and 58 ± 7 kJ mol^{-1}, at 0.60 V and 0.70 V respectively, current densities must be taken 14 s after the potential step during CAs to obtain E_{app} values of 36 ± 5 and 58 ± 8 kJ mol^{-1}, respectively. Notably, these times during CAs (5 and 14 s) clearly fall within the period where E_{app} exhibits time-dependent behavior (*cf.* Fig. 1(g-h)). This correspondence demonstrates that CVs measurements, even when initial conditions and scan directions are well-controlled and varied, may not be appropriate for determining E_{app} values. Conversely, when E_{app} is determined from the current densities at 600 s, corresponding to steady-state conditions, a value of 96 ± 11 kJ mol^{-1} is obtained. This value closely aligns with the *ca.* 123 kJ mol^{-1} determined as the activation energy value for the oxidation of CO_{ad} to CO_2 (r_{6c}) on a Pt(1 0 0) surface [43]. This alignment suggests that this particular reaction step remains sufficiently slow until 0.70 V to act as a rate-limiting step without entirely poisoning the surface at this potential. Nonetheless, the existence of concurrent parallel pathways during the MEOR also influences the reaction kinetics [20] and results in lower E_{app} than the determined for the CO oxidation reaction alone.

The experimental findings discussed above provide strong support for the numerical results previously reported using a model system [40], confirming the superior suitability of CAs for assessing E_{app} values. This emphasizes the reliability and relevance of E_{app} values determined under steady-state conditions for evaluating the intrinsic electrocatalytic activity of electrodes. Additionally, under steady state the reaction rate stabilizes, and the concentration of reaction intermediates remains constant over time, although they may show a temperature dependence [25]. Consequently, variations in the current due to transient poisoning processes can be safely disregarded at all temperatures. This is in contrast with the E_{app} values determined under transient conditions, which are inherently subject to significant fluctuations during surface poisoning. For instance, the lower E_{app} values observed for the MEOR at potential values below 0.70 V and non-steady-state conditions may initially be misconstrued as a barrier to overcome. However, driving the reaction beyond the point of electrode surface poisoning demands a greater amount of energy input. Considering these limitations, the interpretation of E_{app} values obtained from CVs measurements and at short times during CAs may not be suitable, especially when the goal is

to extract information regarding the reaction steps governing the reaction kinetics, which is crucial for designing materials tailored for enhanced electrocatalytic activity within energy conversion systems.

3.2. Temperature-dependent kinetics: potential oscillations

The MEOR on Pt(100) under current control has revealed the spontaneous occurrence of potential oscillations [23,24], providing a way to gain more detailed insight into surface processes compared to conventional approaches [19]. In this sense, to comprehensively investigate the effect of temperature on the MEOR, an evaluation of the oscillatory dynamics was also conducted at various temperatures. Fig. 2

(a-f) show the galvanodynamic profiles, illustrating the potential recorded during current scans, at temperatures ranging from 10 to 35 °C. These profiles allow for the identification of the current range in which oscillations emerge. Broadly, the current density at which the electrochemical response loses stability, initiating oscillatory dynamics, increases with the temperature. The oscillatory behavior persists until a critical current density is reached, causing the electrode potential to abruptly rise beyond 1.0 V to maintain the applied current density. In all temperatures studied, the oscillations that appear in the onset current are simple ones, characterized by a high frequency, low-amplitude, and harmonic behavior. At higher applied current densities, these simple patterns evolve into mixed-mode oscillations, which exhibit large
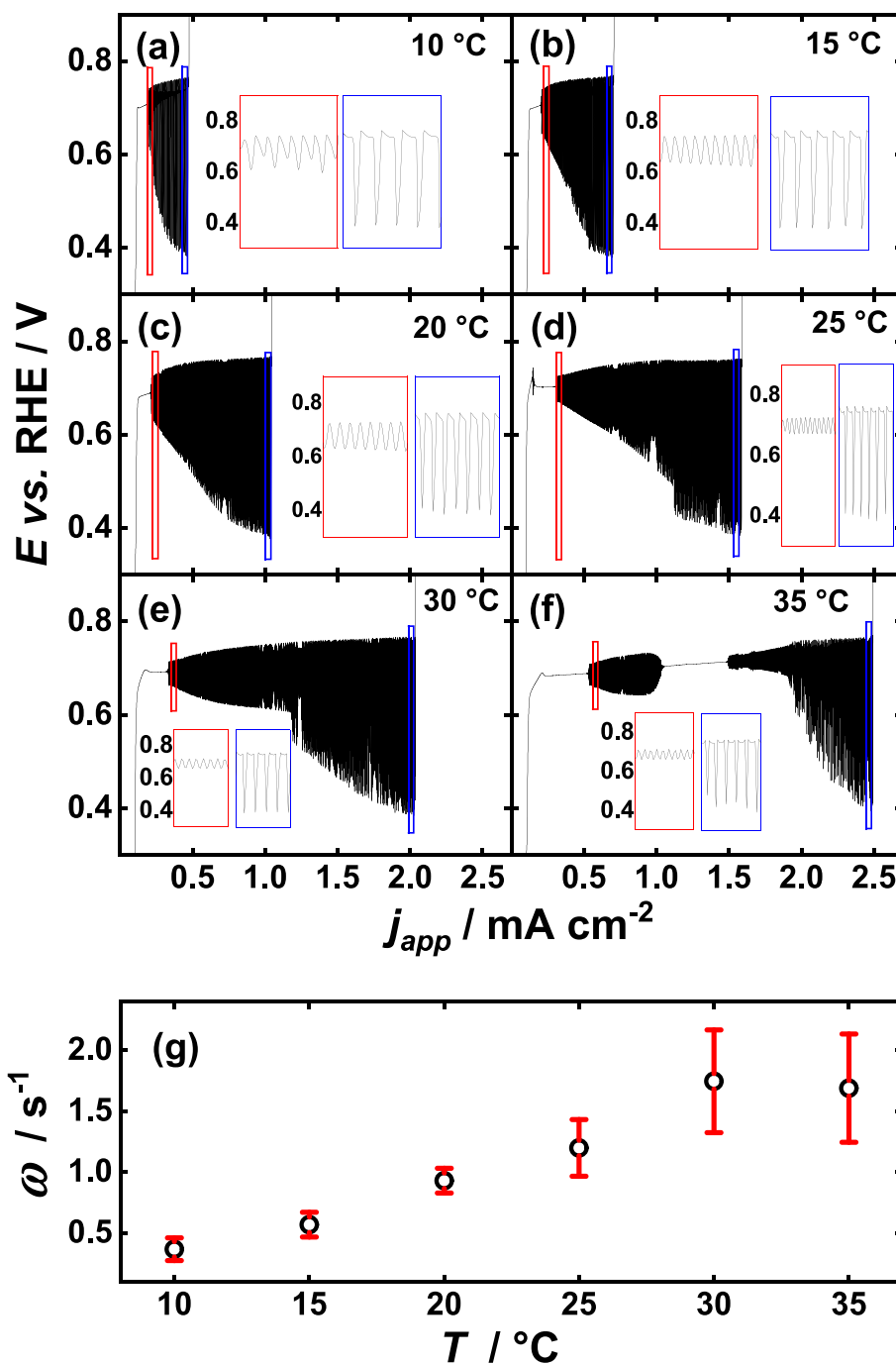

Fig. 2. (a-f) Galvanodynamic profiles of the MEOR on Pt(100) in 0.5 mol L^{-1} HClO$_4$ + 0.5 mol L^{-1} CH$_3$OH at scan rate 2.0 μA s^{-1} cm^{-2} and different temperatures (the boxes correspond to expanded areas within the oscillatory window); (g) average frequency of oscillations during the galvanodynamic scans at different temperatures in Figures (a-f).

amplitudes and low frequencies, interspersed with smaller modulations occurring around 0.73 V (see insets in Fig. 2(a-f)).

As already mentioned, changes in the recorded potential are usually linked to variations in surface coverage by blocking species. However, it is important to note that the mechanisms underlying the single and mixed-mode oscillations are fundamentally different, resulting in the co-existence of two distinct oscillators. Firstly, the oscillator responsible for simple oscillations (oscillator 1) consists of a series of processes in which an increase in potential promotes the formation of OH_{ad} species (r_{5c}), subsequently blocking the electrode surface. This surface poisoning causes a further potential increase as part of an autocatalytic process to maintain the applied current. However, when the potential reaches a critical value, the blocking species reacts with other blocking species (*e. g.*, CO_{ad}) releasing electrons and generating available surface sites to continue the oxidation process (r_{6c}). Consequently, the potential required to sustain the applied current decreases. As the potential decreases, the surface begins to poison once again, initiating the entire process anew and resulting in the observed simple oscillations [21,22,25].

On the other hand, in the case of mixed-mode oscillations, the drop in the potential from high to lower values has been associated with a periodic re-establishment of the methanol concentration in the double layer [23]. These oscillations are predominant at prolonged times and higher applied current densities, conditions in which a deficit of methanol at the reaction plane near the electrode surface may emerge [23]. Under extended time conditions, methanol consumption increases and partially oxidized by-products accumulate, potentially hindering the approach of fresh methanol molecules to the electrode surface [44]. This aligns with previous reports associating mixed-mode oscillations with the presence of soluble by-products [45]. In the latter case, higher applied current densities imply accelerated methanol consumption, leading to a deficit at the electrode surface. The reduced availability of reactant at the surface results in a decrease in the amount of adsorbed reaction intermediates and, consequently, a decrease in the total surface coverage by poisoning species. This lower coverage leads to a decrease in the potential required to sustain the applied current density until a minimum value at which the adsorption of methanol is favored, *i.e.*, around 0.4 V on this particular surface [34]. Once the methanol concentration at the electrode surface is re-established, reaction intermediates are formed, increasing the coverage, and, consequently, the electrode potential. At higher potentials, surface processes occur between adsorbed species [25] causing fluctuations in the potential, until a methanol deficit occurs again, initiating the entire cycle anew. These processes constitute the second oscillator.

Now that the origins of the two primary oscillatory modes during the MEOR have been elucidated, the prevalence of mixed-mode oscillations at lower temperatures (Fig. 2(a-f)), to the extent that at 10 °C, simple oscillations nearly disappear, suggest that during the oscillatory behavior, the direct oxidation pathways involving formaldehyde, methyl formate or formic acid intermediates become more prominent at low temperatures. This phenomenon can be attributed to the reduced energy available for driving reactions and the elevated activation energy required for CO_{ad} oxidation to CO_2. Consequently, methanol oxidation via the CO_{ad} pathway at these temperature conditions may rapidly lead to electrode poisoning, triggering an increase in electrode potential to sustain the applied current and thus the suppression of the oscillations. However, pathways involving the production of soluble by-products yield fewer electrons per molecule of methanol being oxidized compared to the number of electrons generated in the production of CO_2 through the CO_{ad} pathway. This preference for these oxidation pathways at lower temperatures serves to limit the stability of oscillations at higher applied current densities, resulting in the contraction of the oscillatory window. In essence, lower temperatures correspond to a narrower existence region of the potential oscillations.

On the other hand, as temperature increases, the gradual emergence of the oscillator 2 at prolonged times becomes more distinctive. For

example, at 35 °C (Fig. 2(f)), simple oscillations are predominant, which are separated by a window of non-oscillatory behavior before transitioning into mixed-mode oscillations. This suggests that at higher temperatures, processes comprising oscillator 1 are favored. However, at higher applied currents, the consumption of methanol plays a crucial role in causing the emergence of mixed-mode oscillations. Furthermore, an increase in temperature also leads to an increase in the average frequency of oscillations (ω) during the galvanodynamic scan (Fig. 2(g)), indicating that the rates of poisoning also increase. This phenomenon will be further explored through experiments conducted under galvanostatic conditions.

To gain a deeper understanding of the correlation between oscillatory behavior and the underlying reaction mechanism, it is advantageous to analyze the system under galvanostatic conditions. Under these conditions, changes in potential can be directly correlated with the processes occurring to maintain the constant applied current. Since the region of applied current where spontaneous oscillatory behavior emerges varies with different temperatures (Fig. 2), assessing the effect of temperature on the MEOR dynamics while excluding the influence of applied current is imperative. To achieve this, a normalization process was employed in relation to the window of the oscillatory behavior shown in Fig. 2(a-f) at each temperature according to equation (1) [46]:

$$j_N = \frac{j_{app} - j_{osc,i}}{j_{osc,f} - j_{osc,i}} \tag{1}$$

where j_N denotes the normalized current density, j_{app} denotes the applied current, and $j_{osc,i}$ and $j_{osc,f}$ denote the initial and final currents that define the oscillatory potential region, respectively, in the galvanodynamic sweeps in Fig. 2(a-f). As previously stated, simple oscillations prevail at lower applied current densities, which, during a current density step, evolve into mixed-mode oscillations at prolonged time intervals. Therefore, to isolate the temperature effect on the MEOR, experiments were conducted under a j_N value of 0.3, corresponding to the beginning of the oscillatory window. Analyzing the oscillatory profile at low values of j_N, *i.e.*, near the Hopf bifurcation, allows for a more controlled assessment of the processes underlying simple and mixed-mode oscillations. This is in contrast to the high j_N values, far from the bifurcation, where the processes are overlapped, making the analysis difficult and obtaining reliable data on MEOR more challenging.

3.2.1. Overall oxidation under oscillatory regime

The region of the time-series corresponding to the onset of oscillations at $j_N = 0.3$ are shown in Fig. 3. For a complete view of the entire time-series, refer to Figure S3 in the SI. An initial examination reveals that with each temperature increase of 5 °C, the waveform of the oscillations is only minimally affected, while the effect of temperature is mainly reflected in frequency and amplitude. Since the maximum potential achieved during the oscillations remains nearly unaffected by temperature (only a small diminution is observed for 35 °C), a decrease in the minimum potential during the potential cycles observed for low temperatures reflects an increase in the amplitude. This characteristic behavior has been associated with higher efficiency in terms of the mean potential (E_{mean}) required to sustain a specific applied current density [47]. In other words, when E_{mean} is higher, the efficiency decreases, whereas a lower E_{mean} value yields a higher efficiency, as the overpotential decreases. However, even with the expanded amplitude, the E_{mean} values, determined by the ratio of the area under the curve to the time in the same time window [47], remain relatively unchanged across varying temperatures (indicated by the blue lines in Fig. 3). This observation implies that the increase in oscillation amplitude does not imply an enhance in the overall efficiency of the system. The absence of a discernible E_{mean} dependency on temperature, despite amplitude changes, can be attributed to a compensatory effect. As temperature decreases, the expanded amplitude coincides with changes in the waveform of the oscillations, causing the electrode potential to remain
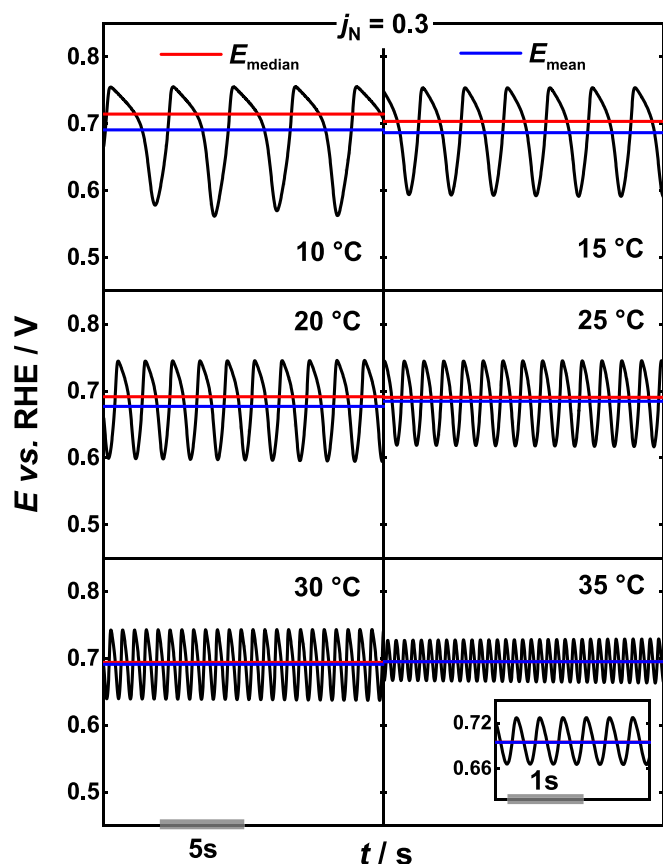
Fig. 3. Potential time series corresponding to the onset of oscillatory behavior during the MEOR on Pt(1 0 0) in 0.5 mol L^{-1} HClO$_4$ + 0.5 mol L^{-1} CH$_3$OH at applied normalized current density, j_N, of 0.3 and different temperatures. The $j_N = 0.3$ corresponds to 0.27 mA cm^{-2} (10 °C), 0.36 mA cm^{-2} (15 °C), 0.46 mA cm^{-2} (20 °C), 0.69 mA cm^{-2} (25 °C), 0.84 mA cm^{-2} (30 °C), and 1.12 mA cm^{-2} (35 °C). The red and blue lines correspond to the median and mean potential in the oscillatory window, respectively. (For interpretation of the references to colour in this figure legend, the reader is referred to the web version of this article.)

at higher values for a longer time. Although this effect is nearly imperceptible when observed within 5 °C intervals, the change becomes evident when comparing the profiles at 10 and 35 °C in Fig. 3. Here, it is evident that oscillations become more symmetric around the x-axis as temperature increases.

The evaluation of the potential values at which the electrode remains for a longer time can be effectively achieved using the median value (E_{median}) within each oscillatory region displayed in Fig. 3. As a statistical measure, this value serves as a valuable metric because it accurately bisects the range of potential values at which the electrode spends half of its time during oscillations. The red lines displayed in Fig. 3 demonstrate that the E_{median} is higher than E_{mean}, particularly at lower temperatures, reflecting that the electrode remains for longer periods at high potentials. As the temperature increases, E_{median} progressively decreases until, at 35 °C, E_{median} and E_{mean} converge at the same value. To account for the varying amplitude at different temperatures and isolate the temperature-dependent effects on E_{median}, a normalization procedure was employed. The normalized median, $\overline{E}_{median}$, was calculated using the equation (2),

$$\overline{E}_{median} = \frac{E_{median} - E_{min}}{E_{max} - E_{min}} \tag{2}$$

where E_{min} denotes the minimum potential reached during the oscillations and E_{max} represents the maximum potential reached during the

same oscillatory cycles.

After the normalization process, $\overline{E}_{median}$ exhibits a consistent trend of progressive decrease with increasing temperature. Once E_{mean} is normalized similarly, both values converge to a value near 0.5, resulting in a ratio of 1 between the two values (for details, see Figure S4 in the SI). This means that at higher temperatures, the time that the electrode potential remains at higher values is equal to the time that the electrode potential remains at lower values, resulting in more symmetrical oscillations. This observation underscores that the minimum potential reached during the oscillations cannot be directly, a priori, linked to E_{mean}. Specifically, the assumption that lower minima are indicative of lower E_{mean} and subsequently correlate to system efficiency does not hold true. As shown here, for asymmetric oscillations where E_{median} exceeds E_{mean}, considering the waveform characteristics is of paramount importance. Consequently, the calculation of E_{mean} should be consistently applied to evaluate the system's efficiency. On the other hand, for both symmetric oscillations ($E_{median} = E_{mean}$) in which the maximum potential remains relatively constant, and asymmetric oscillations in which the potential predominantly remains at lower potential regions ($E_{median} < E_{mean}$), as observed during the formic acid electro-oxidation reaction (FAEOR) [41,48,49], lower minimum values reached during the oscillations can indeed be linked to E_{mean} and, consequently, to overall efficiency. The next section will discuss the origin of the processes responsible for the waveform alteration of the simple oscillations in Fig. 3, in alignment with the impact of temperature on the reaction pathways.

3.2.2. Short-term behavior: Simple oscillations

As previously mentioned, changes in electrode potential are intricately related to changes in the total coverage of species blocking the electrode surface. Specifically, an increase in potential corresponds to an increase in the total electrode coverage, while a decrease indicates the release of active sites (see Figure S5) [25]. From the perspective of E_{mean}, it can be inferred that the mean total coverage of the electrode surface remains nearly constant during temperature changes, at least during the occurrence of the processes that generate simple oscillations. Nonetheless, it is essential to recognize that the relative proportions of the various species at the electrode surface may change at different temperatures. This can influence the rates of the various poisoning and site-release processes, impacting the waveform and, consequently, the E_{median} of the oscillations. In order to deepen the analysis of the processes underlying the oscillations, in particular those leading to the emergence of simple oscillations, their rates, which are given by the derivative of potential with respect to time (dE/dt) can be studied.[47,50] Explicitly, the region where $dE/dt > 0$ is indicative of the poisoning rate, whereas $dE/dt < 0$ is linked to site release rate. This derivative, therefore, provides a more intricate view of the kinetics at which the processes causing the oscillations develop.

Fig. 4(a-f) present the derivatives calculated from the oscillatory profiles in Fig. 3 for a single oscillation period at each temperature. As one would anticipate according to the Arrhenius dependence, an increase in temperature should lead to an acceleration of all reaction steps due to the higher energy input. This trend is indeed observed within the temperature range of 10 to 30 °C, as evidenced by the increasing magnitude in the maximum value of the derivative and the overall rate of poisoning and site release shown in Fig. 4(g). To quantify the global poisoning rate, these values were determined by calculating the ratio between the amplitude of the oscillations ($\Delta E_{osc} = E_{max} - E_{min}$) and the time taken for the electrode to transition from the minimum to the maximum potential during oscillations (Δt_{max}). Similarly, for the global rate of site release, the amplitude (ΔE_{osc}) corresponds to $E_{min} - E_{max}$, and the time corresponds to the duration required for the electrode to return from the maximum to the minimum potential (Δt_{min}) (for details see Figure S6). Within the temperature range of 10 to 30 °C, Fig. 4(a-e) not only illustrate an increase in the magnitude of the derivatives but also
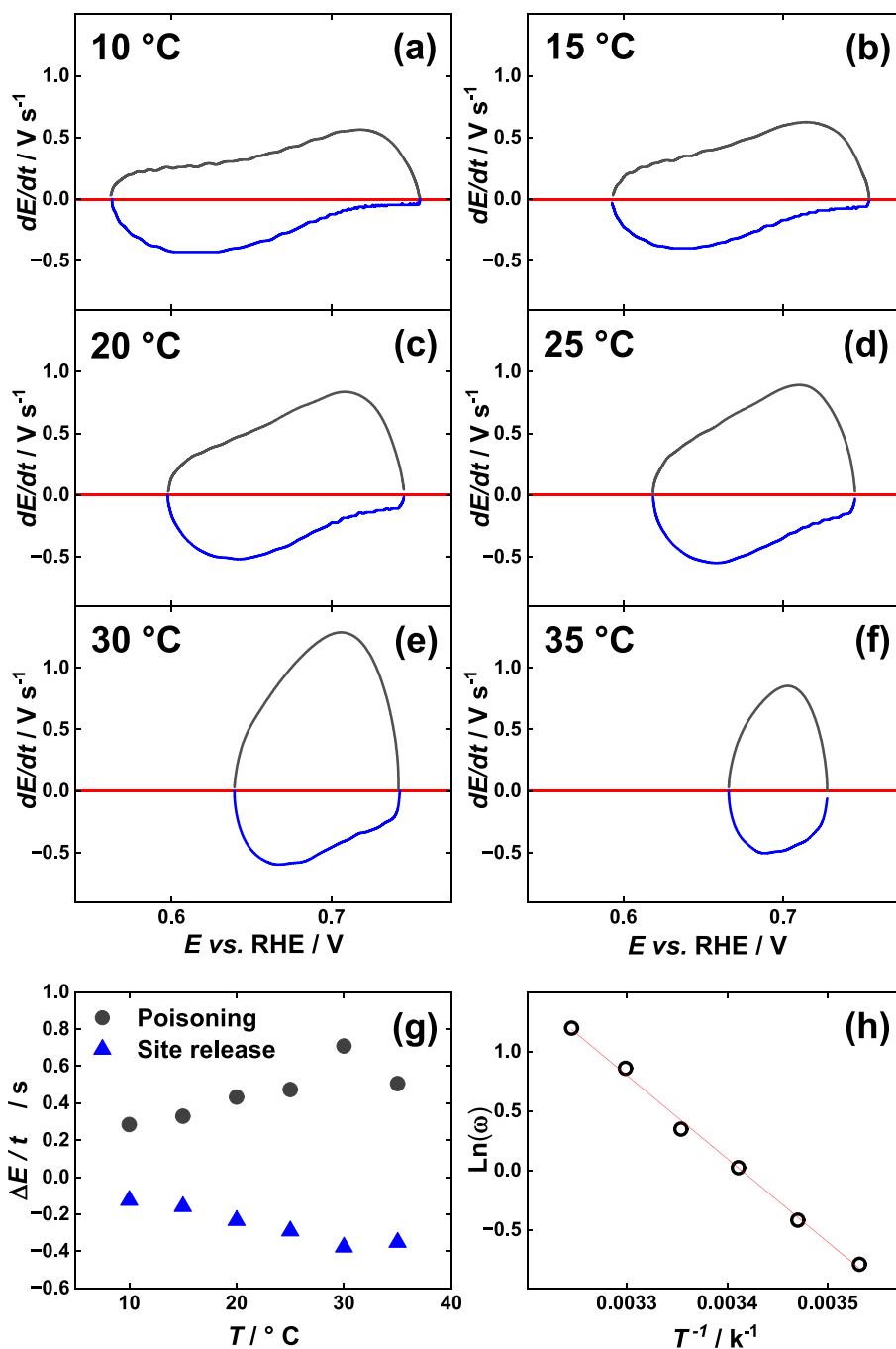
Fig. 4. (a-f) dE/dt profiles corresponding to a single oscillation cycle for the galvanostatic time series of Fig. 4; (g) overall rate of poisoning and site release processes; (h) $\ln\omega$ vs. $1/T$ plot for oscillations in Fig. 3.

demonstrate that higher temperatures impact the shape of the curves. Specifically, at lower temperatures, the dE/dt vs. E curves appear to be a convolution of distinct processes occurring at different rates across an extended potential window. With increasing temperature, the peak of the curve shifts towards higher potential values, and the curve shapes evolve into a single peak shape, signifying a predominant influence of processes within a narrower potential window. In essence, this means that the rates of the processes at different potential ranges are distinctly affected by changes in temperature, such that, despite an overall acceleration, the contribution of processes occurring at low potentials to the oscillatory kinetics seems to be suppressed with increasing temperature.

Focusing on the negative part of the dE/dt vs. E curves, which

corresponds to the rate of site-releasing processes, for example, at 10 °C, the maximum rate is observed at around 0.61 V. According to the reaction mechanism outlined in Scheme 1, the reaction steps within the reaction mechanism responsible for release sites primarily involve the steps related to product formation (r_{2b}, r_{5d}, r_{5a}, r_{-6a}, r_{8a}, and r_{6c}). It is worth noting that, while reaction step r_{7a} also liberates sites, this requires additional vicinal sites for it to proceed (for a detailed discussion of the reaction mechanism, refer to reference [25]). Among the product formation steps, those that are kinetically easier to occur, i.e., those that can occur at lower potential values, are associated with the formation of soluble byproducts like formaldehyde, methyl formate, and formic acid (r_{2b}, r_{5d}, and r_{5a}). These results suggest that at lower temperatures, the reaction pathways leading to the formation of these byproducts (direct

reaction pathways) are favored over the reaction pathway involving the CO_{ad}. It is worth clarifying that the formation of CO_{ad} species is almost inevitable, and a fraction of the surface is always partially occupied by this intermediate. Therefore, during an oscillatory cycle under conditions of reduced energy input, *i.e.*, relatively low temperature, the potential remains elevated for a longer time to promote the oxidation of CO_{ad} species, which occurs more slowly. Consequently, there is a slower decrease of the potential during oscillations due to the low site release rate, resulting in a higher E_{median} value, as previously shown. However, when a fraction of surface sites becomes available, the total coverage, and subsequently the electrode potential, decreases. At this point, methanol oxidation occurs at higher rates, primarily via direct reaction pathways, resulting in a more pronounced negative derivative at lower potentials. Since direct pathways are favored, more active sites are released than if the reaction occurred via CO_{ad}, leading to a less temporal coverage of the electrode surface. This results in lower E_{min} and a higher amplitude during the oscillatory behavior. This is particularly significant because the system autonomously prefers the direct reaction pathways to prevent the electrode poisoning, underscoring the advantage of working under oscillatory conditions [47,50,51].

As the temperature increases to 35 °C, there is a deviation from the trend observed in the range between 10 and 30 °C, and the magnitude of the derivative no longer increases (Fig. 4(a-f)). This observation is consistent with the behavior of the global rates of poisoning and site release processes, where the maximum rate is observed at 30 °C (Fig. 4 (g)). However, Fig. 4(f) shows that despite this, the shape change in the curve with increasing temperature, shifting the maximum and narrowing the curve to higher potentials, is still maintained. The high and narrow potential window in which these processes occur suggests that the most energy-demanding step, which involves the CO_{ad} and OH_{ad} species (reaction step r_{6c}), predominantly governs the site release processes, while their formation likely dominates the poisoning of the electrode surface, thereby shaping the dE/dt *vs.* E curve at 35 °C. This also explains the decrease in the magnitude of the rates of poisoning and site release processes, given the higher activation energy and the slower kinetics of the reaction step r_{6c} in comparison to the direct pathways [25,44]. Having identified the processes occurring at the two extremes of the temperature range, it can be deduced that the changes in the curve shape during the transition from low to high temperatures correspond to both processes, encompassing byproducts formation alongside CO_2 production.

The decrease in the amplitude of the oscillations with increasing temperature may be attributed to the accelerated formation rate of CO_{ad}, leading to the re-poisoning of the surface before the potential has a chance to decrease to lower values. Furthermore, the formation of OH_{ad} species, primarily occurring at higher overpotentials, must be favored to oxidize the CO_{ad} in the reaction step r_{6c}. This, in turn, prevents the electrode potential from decreasing to lower values, resulting in the observed reduction in amplitude. This is in line with our earlier discussion, wherein it was highlighted that elevated temperatures do not significantly enhance the formation of OH_{ad} species on the Pt(100) surface [39]. However, even though elevated temperatures promote the formation of CO_{ad} and higher potential values facilitate OH_{ad} formation, the E_{mean} value, which is directly linked to the average total coverage, is not significantly affected. This implies that the fraction of active sites being occupied by intermediates involved in the direct oxidation pathways, the reaction pathways that lead to the formation of by-products, must decrease, hindering these reaction pathways. Consequently, it can be established that, at lower temperatures, the direct reaction pathways are favored, with their intermediates making a substantial contribution to the total surface coverage. On the other hand, as temperature increases, these reaction pathways seem to be suppressed and lose significance, while the indirect oxidation pathway, via the CO_{ad} intermediate, becomes the dominant process governing the reaction kinetics. This behavior suggests that the system autonomously selects the oxidation pathways to avoid complete poisoning of the electrode

surface. This mechanism is reminiscent of kinetic and thermodynamic control, which govern the reaction kinetics at low and high temperatures, respectively.

Changes in the processes contributing to the oscillatory behavior at the different temperatures lead to a reduction in both Δt_{max} and Δt_{min} (Figure S7). Thus, the increase in temperature results in a remarkable sevenfold reduction in the oscillation period and a subsequent increase in the frequency of the potential oscillations. This implies that higher temperatures lead to more cycles of self-cleaning on the electrode surface, where self-cleaning comprises a full cycle of poisoning and site-release processes. This finding holds significant implications for DMFCs and electro-reforming devices utilizing methanol at high temperatures, as it helps prevent the poisoning of electrocatalysts. The self-cleaning processes can be compared to a series of autocatalytic reaction bursts occurring at a certain frequency, effectively treating the entire process as a monomolecular reaction characterized by a rate constant equivalent to the oscillation frequency (ω) [52]. Consequently, plotting $\ln\omega$ against $1/T$ in Fig. 4(h) allows to determine the activation energy for the oscillatory behavior (E_{app}^{osc}), which equates to 58 ± 2 kJ mol^{-1}. This value signifies the sensitivity of ω to temperature variations, with its positive value indicating that the oscillation frequency increases with higher temperatures, at least within the studied temperature range. It has been proposed that an increase in the reaction rates of steps within the positive feedback loop (processes that poison surface with blocking species) will lead to an increase in the oscillatory frequency, while an increase in the reaction rates of steps within the negative feedback loop (processes that release surface sites) will decrease the frequency [53]. This aligns with the observed increase in frequency of oscillations with temperature and the positive value of E_{app}^{osc}. This is because the temperature increase predominantly enhances the kinetics of surface poisoning (negative feedback loop – reaction steps represented by the red arrows in Scheme 1) over the kinetics of site release (positive feedback loop - reaction steps represented by the blue arrows in Scheme 1), which is supported by the steeper slope of $\Delta E_{osc}/t_{max}$ (poisoning process) compared to $\Delta E_{osc}/t_{min}$ (site release process) as function of temperature in Fig. 4(g).

It is important to note that increases in frequency should not be directly linked to a proportional increase in the rates of single reaction steps constituting the feedback loops driving these oscillations. This is because, during the oscillations, the reaction steps may contribute differently to changes in frequency, even in some reactions, such as that of FAEOR, some reaction steps may generate the opposite effect of reducing the oscillation frequency as temperature increases. Such a phenomenon is referred to as the antagonistic balance of opposing reactions [54]. This balance can give rise to situations where E_{app}^{osc} equals zero ($E_{app}^{osc} = 0$), signifying compensation phenomena where frequency remains relatively unaltered despite temperature variations. Alternatively, E_{app}^{osc} can take negative values ($E_{app}^{osc} < 0$), indicating over-compensation phenomena, where oscillatory processes slow down as temperature increases [41]. Therefore, to discern the influence of the rate of each elementary step on the frequency change caused by temperature increases and its contribution to the total value of E_{app}^{osc}, numerical approaches, such as microkinetic modeling, can be very useful [41].

3.2.3. Long-term behavior: Mixed-mode oscillations

During prolonged periods of the current step in a galvanostatic experiment, the simple oscillations gradually transition into mixed-mode oscillations. As mentioned earlier, the drop to low potential values (around 0.40 V) has been associated with a cyclic re-establishment of the methanol concentration at the electrode surface [23], while the fluctuations in potential around 0.73 V can be linked to changes in the coverage of adsorbed species on the electrode surface [25] (as discussed at the beginning of section 3.2). Fig. 5 depicts the final section of the time series presented in Figs. 3 and S3 at $j_N = 0.3$, just
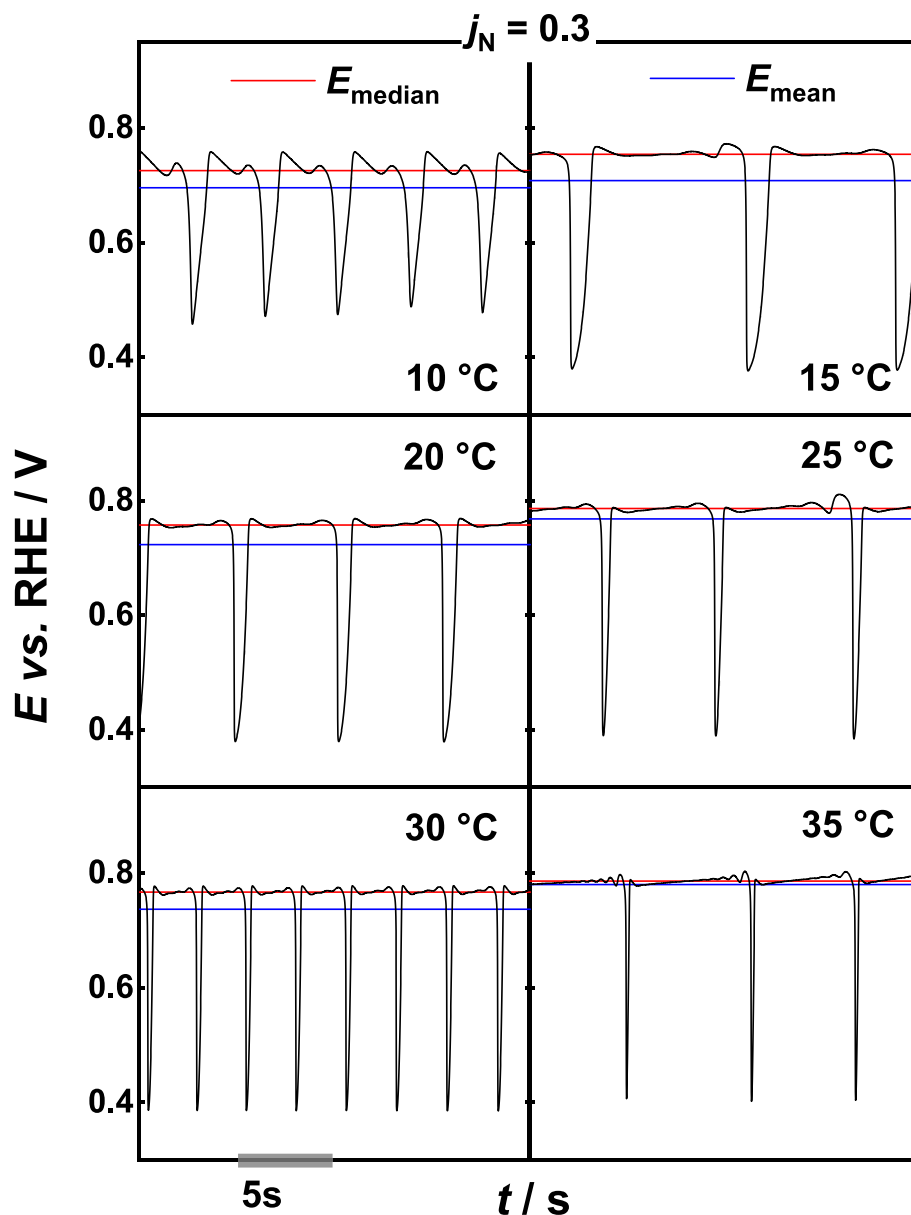
Fig. 5. Potential time series corresponding to the end of oscillatory behavior during the MEOR on Pt(1 0 0) in 0.5 mol L^{-1} HClO$_4$ + 0.5 mol L^{-1} CH$_3$OH at applied normalized current density, j_N, of 0.3 and different temperatures. The j_N = 0.3 corresponds to 0.27 mA cm^{-2} (10 °C), 0.36 mA cm^{-2} (15 °C), 0.46 mA cm^{-2} (20 °C), 0.69 mA cm^{-2} (25 °C), 0.84 mA cm^{-2} (30 °C), and 1.12 mA cm^{-2} (35 °C). The red and blue lines correspond to the median and mean potential during the oscillatory window, respectively. (For interpretation of the references to colour in this figure legend, the reader is referred to the web version of this article.)

before the potential rises to values exceeding 1.0 V, where these mixed-mode oscillations predominantly occur. In contrast to the simple oscillations observed at the beginning of the time series, which displayed a clear trend in the changes of amplitude, frequency, and waveform (Fig. 3), the mixed-mode oscillations display nearly constant amplitude and no clear trend in oscillation frequency at different temperatures. However, two main trends in the oscillation features become apparent with increasing temperature. First, the region where the potential drops to *ca.* 0.40 V becomes narrower, and second, the fluctuations in potential at around 0.73 V decrease in magnitude as temperature rises (Fig. 5).

In the first case, the narrowing of the potential drop, meaning a shorter time during which the electrode remains at a low potential, can be attributed to the increased rate of the methanol concentration re-establishment cycle. This observation is supported by the increased magnitude of the *dE/dt vs. E* curves in Fig. 6, for both negative and positive values, corresponding to site release and poisoning processes, respectively. These trends provide evidence of the enhanced rate of

these processes with increasing temperature. As the methanol re-establishment causes the electrode potential to move over a wide potential window, the derivative plot exhibits a broadband shape (Fig. 6). Focusing on the negative part of the curve, a similar trend as that observed in the derivatives of the oscillatory patterns at shorter times (Fig. 4(a-f)) becomes apparent, with the maximum of the curve shifting to higher potential values as the temperature rises. This indicates that, as discussed previously, the increase in temperature favors the reaction pathway via CO$_{ad}$ (r_{6c}), which requires a higher overpotential to occur. At the point where the electrode reaches its lowest potential, a significant reduction in the coverage of the electrode surface by blocking species is expected. Therefore, in the case of the positive part of the *dE/dt vs. E* in Fig. 6, the processes responsible for the increase in electrode potential at this stage can be associated with methanol adsorption and subsequent steps that require more active sites for the formation of reaction intermediates. Therefore, the enhanced rates of these different steps contribute to the multi-peak shape observed in the
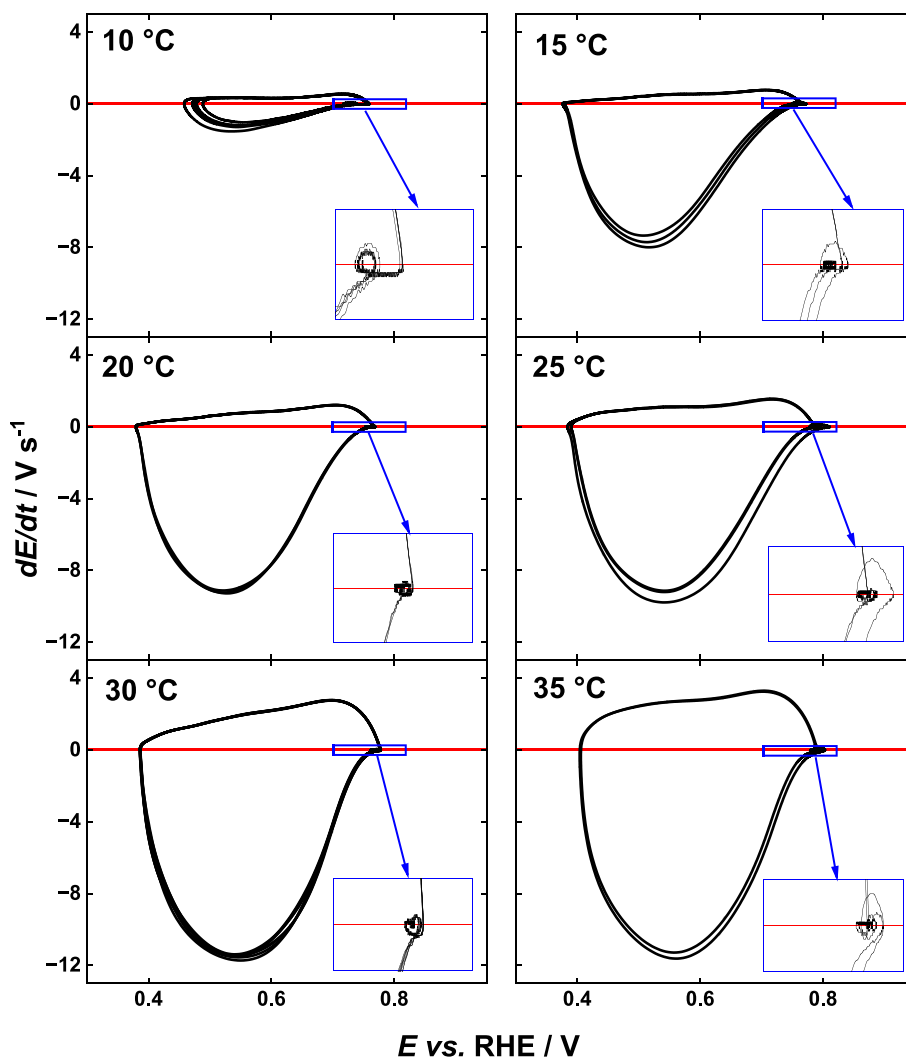
Fig. 6. dE/dt *vs.* E curves corresponding to oscillatory behavior in Fig. 5.

$dE/dt > 0$ curves, along with their increased magnitude at higher temperatures.

Regarding the fluctuations in potential at around 0.73 V, Fig. 5 reveals that at 10 °C, the amplitude of the potential modulations is the highest. This behavior is expected because, at lower temperatures, the formation of reaction by-products is favored, which can influence the rate of formation and consumption of CO_{ad} species, particularly the direct oxidation pathway via methyl formate, causing these potential variations [25]. As the temperature increases, the rates of poisoning and site release, caused by adsorbed species, accelerate to the point where these rates nearly equilibrate, resulting in the decreased amplitude of the modulations at around 0.73 V. However, around the cycle of methanol re-establishment, just before the electrode potential drops and just after it rises again, the deficit and subsequent re-establishment of the methanol concentration changes the rate of CO_{ad} formation. This leads to a decoupling of the rates of poisoning and site release processes, revealing the potential undulations around the methanol re-establishment cycle. However, these become less pronounced in the middle of mixed-mode oscillations as the rates tend to equilibrate. The two phenomena together, increasing the rate of methanol concentration re-establishment and favoring the CO_{ad} pathway with rising temperature, lead to an increase in the mean coverage of the electrode during the oscillations, resulting in higher E_{mean} and E_{median} values as temperature increase. It is worth noting that this increase in the electrode potential necessary to maintain the applied current, might result in decreased

voltaic efficiency at higher temperatures. Therefore, to increase the voltaic efficiency of the MEOR under oscillatory conditions, while favoring the formation of the most oxidized product (CO_2), mass transfer must be enhanced, avoiding concentration gradients that lead to the suppression of mixed-mode oscillations despite their higher amplitude. These findings offer valuable insights into comprehending the temperature effect on the MEOR, which is particularly important for guiding the rational design of materials for the MEOR and optimizing the operating temperature of DMFCs and electro-reforming devices to produce H_2 in the presence of methanol in the anodic compartment.

4. Conclusions

The impact of temperature on the kinetics of the methanol electro-oxidation reaction on Pt(1 0 0) has been extensively explored, encompassing both conventional and oscillatory regimes. This thorough investigation enables a more profound analysis, advancing our understanding of the temperature's impact on the reaction mechanism. These insights have been facilitated by precisely controlled single-crystal experiments and previous microkinetic analyses, propelling our comprehension to a more advanced level. Our study notably underscores the limitations of CVs in determining the E_{app}, demonstrating that chronoamperometric measurements under steady-state conditions provide a more dependable approach to determining this critical kinetic parameter. This establishes a robust connection between the electrocatalytic

activity of electrodes and E_{app} values. In our research on the reaction pathways governing the MEOR, a temperature-dependent shift in the dominance of specific oxidation pathways is clearly observed. At lower temperatures, direct oxidation pathways, likely involving methyl formate, formaldehyde, or formic acid intermediates, significantly impact the electro-oxidation of methanol. As the temperature increases, these pathways progressively lose their relevance, ceding dominance to the pathway via CO_{ad} intermediate, particularly becoming the primary reaction pathway. This temperature-induced change is mainly attributed to the reduced energy available to drive the reactions at lower temperatures and the high activation energy required for the oxidation of CO_{ad} to CO_2. This phenomenon resembles a mechanism analogous to kinetic and thermodynamic control, which operate at low and high temperatures, respectively, to avoid complete poisoning of the electrode surface.

Through oscillatory regime measurements, the common assumption that associates lower oscillation minima with lower mean potential, presuming an enhanced voltaic system efficiency is challenged. At short times of oscillatory behavior, the mean potential, and consequently the electro-oxidation efficiency remain almost constant despite temperature variations. This observation is attributed to changes in the ratio of coverage of the reaction intermediates, resulting in compensatory effects between the amplitude and the waveform of the potential oscillations. However, during long-term behavior, when mass transfer phenomena start to play a significant role, increasing the temperature leads to a higher mean potential due to a greater coverage of the electrode surface, which in turn, leads to a decrease in the voltaic efficiency. To favor the formation of the most oxidized product while keeping the mean potential constant, it becomes necessary to operate at higher temperatures, mitigating the concentration gradients to suppress the occurrence of mixed-mode oscillations, even if these oscillations have lower temporal minima in the potential during this dynamic behavior. In summary, our study provides valuable insights into the temperature-dependent dynamics of the MEOR and elucidates how temperature variations affect the underlying steps of the reaction mechanism. These findings hold significant importance for guiding the rational design of materials and optimizing the operating conditions of electrocatalytic systems for energy conversion applications.

CRediT authorship contribution statement

Enrique A. Paredes-Salazar: Writing – original draft, Investigation, Formal analysis, Conceptualization. **Alfredo Calderón-Cárdenas:** Writing – review & editing, Validation, Formal analysis. **Enrique Herrero:** Writing – review & editing, Validation, Supervision, Conceptualization. **Hamilton Varela:** Writing – review & editing, Supervision, Methodology, Conceptualization.

Declaration of competing interest

The authors declare that they have no known competing financial interests or personal relationships that could have appeared to influence the work reported in this paper.

Data availability

Data will be made available on request.

Acknowledgments

Appendix A. Supplementary data

Details of the CV profiles during the MEOR, Arrhenius plots, complete time series of the potential oscillations during the MEOR, plots of $\overline{E}_{median}$, $\overline{E}_{media}$ and the ratio between these values, and the schematic representation of ΔE_{osc}, Δt_{max} and Δt_{min}, and their values at different temperatures during the potential oscillations. Supplementary data to this article can be found online at https://doi.org/10.1016/j.jcat.2024.115402.

References

[1] Z.W. She, J. Kibsgaard, C.F. Dickens, I. Chorkendorff, J.K. Nørskov, T.F. Jaramillo, Combining theory and experiment in electrocatalysis: insights into materials design, Science (80-.) 355 (2017) 1–12, https://doi.org/10.1126/science.aad4998.

[2] F.N. Al-Rowaili, A. Jamal, M.S. Ba Shammakh, A. Rana, A review on recent advances for electrochemical reduction of carbon dioxide to methanol using metal-organic framework (MOF) and non-MOF catalysts: challenges and future prospects, ACS Sustain. Chem. Eng. 6 (2018) 15895–15914, https://doi.org/10.1021/acssuschemeng.8b03843.

[3] Methanol Institute, Renewable methanol, (n.d.). https://www.methanol.org/renewable/ (accessed December 11, 2023).

[4] J.M. Léger, Mechanistic aspects of methanol oxidation on platinum-based electrocatalysts, J. Appl. Electrochem. 31 (2001) 767–771, https://doi.org/10.1023/A:1017531225171.

[5] H. Wang, C. Wingender, H. Baltruschat, M. Lopez, M.T. Reetz, Methanol oxidation on Pt, PtRu, and colloidal Pt electrocatalysts: A DEMS study of product formation, J. Electroanal. Chem. 509 (2001) 163–169, https://doi.org/10.1016/S0022-0728(01)00531-9.

[6] J. Ge, H. Liu, Experimental studies of a direct methanol fuel cell, J. Power Sources. 142 (2005) 56–69, https://doi.org/10.1016/j.jpowsour.2004.11.022.

[7] T. Iwasita, Electrocatalysis of methanol oxidation, Electrochim. Acta. 47 (2002) 3663–3674, https://doi.org/10.1016/S0013-4686(02)00336-5.

[8] E.A. Batista, G.R.P. Malpass, A.J. Motheo, T. Iwasita, New insight into the pathways of methanol oxidation, Electrochem. Commun. 5 (2003) 843–846, https://doi.org/10.1016/j.elecom.2003.08.010.

[9] E.A. Batista, G.R.P. Malpass, A.J. Motheo, T. Iwasita, New mechanistic aspects of methanol oxidation, J. Electroanal. Chem. 571 (2004) 273–282, https://doi.org/10.1016/j.jelechem.2004.05.016.

[10] J.L. Cohen, D.J. Volpe, H.D. Abruña, Electrochemical determination of activation energies for methanol oxidation on polycrystalline platinum in acidic and alkaline electrolytes, Phys. Chem. Chem. Phys. 9 (2007) 49–77, https://doi.org/10.1039/b612040g.

[11] Y. Xu, M. Liu, M. Wang, T. Ren, K. Ren, Z. Wang, X. Li, L. Wang, H. Wang, Methanol electroreforming coupled to green hydrogen production over bifunctional NiIr-based metal-organic framework nanosheet arrays, Appl. Catal. B Environ. 300 (2022) 120753, https://doi.org/10.1016/j.apcatb.2021.120753.

[12] A. Sathyaseelan, K. Krishnamoorthy, P. Pazhamalai, N.U.H. Liyakath Ali, S.-J. Kim, Value-added methanol electroreforming coupled with green hydrogen production at the edge interface of 2D boron nanosheets, J. Mater. Chem. a. 11 (2023) 20712–20723, https://doi.org/10.1039/d3ta03513a.

[13] A. Chen, P. Holt-Hindle, Platinum-based nanostructured materials: synthesis, properties, and applications, Chem. Rev. 110 (2010) 3767–3804, https://doi.org/10.1021/cr9003902.

[14] B. Beden, C. Lamy, A. Bewick, K. Kunimatsu, Electrosorption of methanol on a platinum electrode. IR spectroscopic evidence for adsorbed CO species, J. Electroanal. Chem. 121 (1981) 343–347, https://doi.org/10.1016/S0022-0728(81)80590-6.

[15] H. Wang, H.D. Abruña, New insights into methanol and formic acid electro-oxidation on Pt: simultaneous DEMS and ATR-SEIRAS study under well-defined flow conditions and simulations of CO spectra, J. Chem. Phys. 156 (2022), https://doi.org/10.1063/5.0071463.

[16] L. Pérez-Martínez, L.M. Machado de los Toyos, J.J.T. Shibuya, A. Cuesta, Methanol dehydrogenation on Pt electrodes: active sites and role of adsorbed spectators revealed through time-resolved ATR-SEIRAS, ACS Catal. 11 (2021) 13483–13495, https://doi.org/10.1021/acscatal.1c03870.

[17] A.A. Abd-El-Latif, H. Baltruschat, Formation of methylformate during methanol oxidation revisited: the mechanism, J. Electroanal. Chem. 662 (2011) 204–212, https://doi.org/10.1016/j.jelechem.2011.06.031.

[18] H. Wang, T. Löffler, H. Baltruschat, Formation of intermediates during methanol oxidation: a quantitative DEMS study, J. Appl. Electrochem. 31 (2001) 759–765, https://doi.org/10.1023/A:1017539411059.

[19] A. Calderón-Cárdenas, E.A. Paredes-Salazar, H. Varela, A microkinetic description of electrocatalytic reactions: the role of self-organized phenomena, New J. Chem. 46 (2022) 6837–6846, https://doi.org/10.1039/d2nj00758d.

[20] E. Herrero, K. Franaszczuk, A. Wieckowski, Electrochemistry of methanol at low index crystal planes of platinum: an integrated voltammetric and chronoamperometric study, J. Phys. Chem. 98 (1994) 5074–5083, https://doi.org/10.1021/j100070a022.

[21] K K. Krischer, H. Varela, Oxidation of small organic molecules: oscillations and other dynamic instabilities, in: W. Vielstich, A. Lamm, H.A. Gasteier (Eds.), Handb. Fuel Cells Fundam. Tecnol. Appl. Vol. 2 Fuel Cell Electrocatal., Wiley-VCH Verlag, Weinheim, 2010, pp. 1–23. Doi: 10.1002/9780470974001.f206052.

[22] .G. Machado, H. Varela, Kinetic instabilities in electrocatalysis, in: K. Wandelt (Ed.), Encycl. Interfacial Chem. Surf. Sci. Electrochem., Elsevier, Amsterdam, 2018, pp. 701–718. Doi: 10.1016/B978-0-12-409547-2.13369-4.

[23] E.A. Paredes-salazar, E. Herrero, H. Varela, Mass transfer phenomena induced by surface gas flow rate in the hanging meniscus configuration: a case study of the methanol electro-oxidation reaction on Pt(100), Electrochim. Acta 464 (2023) 142917, https://doi.org/10.1016/j.electacta.2023.142917.

[24] B.A.F. Previdello, P.S. Fernández, G. Tremiliosi-Filho, H. Varela, Probing the surface fine structure through electrochemical oscillations, Phys. Chem. Chem. Phys. 20 (2018) 5674–5682, https://doi.org/10.1039/c7cp08028j.

[25] E.A. Paredes-Salazar, A. Calderón-Cárdenas, H. Varela, Microkinetic modeling of the methanol electro-oxidation reaction on platinum, ACS Catal. 13 (2023) 9366–9378, https://doi.org/10.1021/acscatal.3c00838.

[26] E.A. Paredes-Salazar, A. Calderón-Cárdenas, H. Varela, Sensitivity analysis in the microkinetic description of electrocatalytic reactions, J. Phys. Chem. A 126 (2022) 2746–2749, https://doi.org/10.1021/acs.jpca.2c00624.

[27] V. Climent, J.M. Feliu, Surface Electrochemistry with Pt Single-Crystal Electrodes, in: R.C. Alkire, P.N. Bartlett, J. Lipkowski (Eds.), Adv. Electrochem. Sci. Eng. Nanopatterned Nanoparticle-Modified Electrodes, 17th ed., Wiley-VCH Verlag GmbH & Co. KGaA, 2017, pp. 1–57, https://doi.org/10.1002/9783527340934.ch1.

[28] V. Climent, J. Feliu, Single crystal electrochemistry as an in situ analytical characterization tool, Annu. Rev. Anal. Chem. 13 (2020) 201–222, https://doi.org/10.1146/annurev-anchem-061318-115541.

[29] X.H. Xia, T. Iwasita, F. Ge, W. Vielstich, Structural effects and reactivity in methanol oxidation on polycrystalline and single crystal platinum, Electrochim. Acta 41 (1996) 711–718, https://doi.org/10.1016/0013-4686(95)00360-6.

[30] B.A.F. Previdello, P.S. Fernández, G. Tremiliosi-Filho, H. Varela, Oscillatory electro-oxidation of methanol on platinum single crystal electrodes, Electrocatalysis 7 (2016) 276–279, https://doi.org/10.1007/s12678-016-0317-y.

[31] J. Clavilier, R. Faure, G. Guinet, R. Durand, Preparation of monocrystalline Pt microelectrodes and electrochemical study of the plane surfaces cut in the direction of the 111 and 110 planes, J. Electroanal. Chem. 107 (1980) 205–209, https://doi.org/10.1016/S0022-0728(79)80022-4.

[32] N. Garcia-Araez, V. Climent, J.M. Feliu, Temperature Effects on Platinum Single-Crystal/Aqueous Solution Interphases. Combining Gibbs Thermodynamics with Laser-Pulsed Experiments, in: C.G. Vayenas (Ed.), Interfacial Phenom. Electrocatal., 1st ed., Springer New York, NY, New York, 2011, pp. 1–105. Doi: 10.1007/978-1-4419-5580-7_1.

[33] M. Krausa, W. Vielstich, Potential oscillations during methanol oxidation at Pt-electrodes Part 1: experimental conditions, J. Electroanal. Chem. 399 (1995) 7–12, https://doi.org/10.1016/0022-0728(95)04249-0.

[34] D.S. Mekazni, R.M. Arán-Ais, A. Ferre-Vilaplana, E. Herrero, Why methanol electro-oxidation on platinum in water takes place only in the presence of adsorbed OH, ACS Catal. 12 (2022) 1965–1970, https://doi.org/10.1021/acscatal.1c05122.

[35] R. Rizo, J. Fernández-Vidal, L.J. Hardwick, G.A. Attard, F.J. Vidal-Iglesias, V. Climent, E. Herrero, J.M. Feliu, Investigating the presence of adsorbed species

[36] R. Rizo, E. Herrero, V. Climent, J.M. Feliu, On the nature of adsorbed species on platinum single-crystal electrodes, Curr. Opin. Electrochem. 38 (2023) 101240, https://doi.org/10.1016/j.coelec.2023.101240.

[37] M.A. Kamyabi, R. Martínez-Hincapié, J.M. Feliu, E. Herrero, Effects of the Interfacial structure on the methanol oxidation on platinum single crystal electrodes, Surfaces 2 (2019) 177–192, https://doi.org/10.3390/surfaces2010014.

[38] V. Grozovski, V. Climent, E. Herrero, J.M. Feliu, The role of the surface structure in the oxidation mechanism of methanol, J. Electroanal. Chem. 662 (2011) 43–51, https://doi.org/10.1016/j.jelechem.2011.02.032.

[39] V. Climent, R. Gómez, J.M. Orts, J.M. Feliu, Thermodynamic analysis of the temperature dependence of OH adsorption on Pt(111) and Pt(100) electrodes in acidic media in the absence of specific anion adsorption, J. Phys. Chem. B 110 (2006) 11344–11351, https://doi.org/10.1021/jp054948x.

[40] A. Calderón-Cárdenas, E.A. Paredes-Salazar, H. Varela, Apparent activation energy in electrochemical multistep reactions: a description via sensitivities and degrees of rate control, ACS Catal. 10 (2020) 9336–9345, https://doi.org/10.1021/acscatal.0c02359.

[41] A. Calderón-Cárdenas, E.A. Paredes-Salazar, C.A. Mujica-Martinez, R. Nagao, H. Varela, Thorough analysis of the effect of temperature on the electro-oxidation of formic acid, J. Phys. Chem. C 124 (2020) 24259–24270, https://doi.org/10.1021/acs.jpcc.0c08059.

[42] P. Waszczuk, G.Q. Lu, A. Wieckowski, C. Lu, C. Rice, R.I. Masel, UHV and electrochemical studies of CO and methanol adsorbed at platinum/ruthenium surfaces, and reference to fuel cell catalysis, Electrochim. Acta. 47 (2002) 3637–3652, https://doi.org/10.1016/S0013-4686(02)00334-1.

[43] E. Herrero, B. Álvarez, J.M. Feliu, S. Blais, Z. Radovic-Hrapovic, G. Jerkiewicz, Temperature dependence of the COads oxidation process on Pt(111), Pt(100), and Pt(110) electrodes, J. Electroanal. Chem. 567 (2004) 139–149, https://doi.org/10.1016/j.jelechem.2003.12.019.

[44] R. Reichert, J. Schnaidt, Z. Jusys, R.J. Behm, The influence of reactive side products on the electrooxidation of methanol-a combined in situ infrared spectroscopy and online mass spectrometry study, Phys. Chem. Chem. Phys. 16 (2014) 13780–13799, https://doi.org/10.1039/c4cp01229a.

[45] Y. Mukouyama, O. Furuyama, Y. Bundo, H. Okamoto, Separate current range for appearance of potential oscillation during methanol oxidation on platinum, Electrochemistry 82 (2014) 573–577, https://doi.org/10.5796/electrochemistry.82.573.

[46] R. Nagao, I.R. Epstein, E.R. Gonzalez, H. Varela, Temperature (over)compensation in an oscillatory surface reaction, J. Phys. Chem. A 112 (2008) 4617–4624, https://doi.org/10.1021/jp801361j.

[47] M.V.F. Delmonde, L.F. Sallum, N. Perini, E.R. Gonzalez, R. Schlögl, H. Varela, Electrocatalytic efficiency of the oxidation of small organic molecules under oscillatory regime, J. Phys. Chem. C 120 (2016) 22365–22374, https://doi.org/10.1021/acs.jpcc.6b06692.

[48] J.G. Freire, A. Calderón-Cárdenas, H. Varela, J.A.C. Gallas, Phase diagrams and dynamical evolution of the triple-pathway electro-oxidation of formic acid on platinum, Phys. Chem. Chem. Phys. 22 (2020) 1078–1091, https://doi.org/10.1039/c9cp04324a.

[49] A. Calderón-Cárdenas, F.W. Hartl, J.A.C. Gallas, H. Varela, Modeling the triple-path electro-oxidation of formic acid on platinum: cyclic voltammetry and oscillations, Catal. Today. 359 (2021) 90–98, https://doi.org/10.1016/j.cattod.2019.04.054.

[50] F.W. Hartl, A.A. Zülke, B.J. Fonte, H. Varela, Temperature dependence of the evolving oscillations along the electrocatalytic oxidation of methanol, J. Electroanal. Chem. 800 (2017) 99–105, https://doi.org/10.1016/j.jelechem.2016.11.032.

[51] J.A. Nogueira, I.K. Peña Arias, R. Hanke-Rauschenbach, T. Vidakovic-Koch, H. Varela, K. Sundmacher, Autonomous voltage oscillations in a direct methanol fuel cell, Electrochim. Acta 212 (2016) 545–552, https://doi.org/10.1016/j.electacta.2016.07.050.

[52] E. Koros, Monomolecular treatment of chemical oscillation, Nature 251 (1974) 703–704.

[53] P. Ruoff, General homeostasis in period- and temperature-compensated chemical clock mutants formed by random selection conditions, Naturwissenschaften 81 (1994) 456–459, https://doi.org/10.1007/BF01136649.

[54] P. Ruoff, Introducing temperature-compensation in any reaction kinetic oscillator model, J. Interdisiplinary Cycle Res. 23 (1992) 92–99, https://doi.org/10.1080/09291019209360133.